PHARMACIA

Pharmacia 72: 1–13
DOI 10.3897/pharmacia.72.e143192

Research Article

Unraveling the role of hyaluronic acid on the targeting of vinorelbine-loaded NLC for lung cancer

Ali N. Wannas[1], Monther F. Mahdi[2], Nidhal K. Maraie[3]

1 *Department of Pharmaceutics, College of Pharmacy, Mustansiriyah University, Baghdad, Iraq*
2 *Department of Pharmaceutical Chemistry, College of Pharmacy, Mustansiriyah University, Baghdad, Iraq*
3 *Department of Pharmaceutics, College of Pharmacy, Al-Farahidi University, Baghdad, Iraq*

Corresponding author: Ali N. Wannas (aliwennas@uomustansiriyah.edu.iq)

Received 1 December 2024 ♦ **Accepted** 18 February 2025 ♦ **Published** 12 March 2025

Citation: Wannas AN, Mahdi MF, Maraie NK (2025) Unraveling the role of hyaluronic acid on the targeting of vinorelbine-loaded NLC for lung cancer. Pharmacia 72: 1–13. https://doi.org/10.3897/pharmacia.72.e143192

Abstract

Hyaluronic acid (HA) is a naturally occurring mucopolysaccharide that interacts specifically with overexpressed receptors on cancer cells, such as CD44, RHAMM, and LYVE-1, enabling targeted drug delivery to tumors. The present work aims to prepare an activated nanolipid carrier (NLC) using HA as a ligand to enhance the selectivity and safety of parenterally administered vinorelbine (Vn). The preparation method included the chemical conjugation of pegylated-DSPE with HA, followed by the loading of Vn using ultrasonication-homogenization to prepare activated HA-NLC (Vn-loaded HA-NLC). In vitro evaluation for the prepared formulation had a mean particle size of 102 nm, a zeta potential of -44.1 mV, and gave a drug release of 85.23% within 48 hours with an IC50 of 35.7 µg/mL against the lung cancer cell line A549 in comparison to the marketed drug and non-activated Vn-loaded NLC, which gave IC50 values of 45.65 µg/mL and 57.29 µg/mL, respectively. The in vivo study in mice of the Kunming strain included the induction of lung cancer (LL2) xenograft (equivalent to humanized A549), measurement of mice body weight and tumor volume, histopathological study for 4 weeks, and MRI follow-up scan of tumor tissue for 24 hours using SPION as a contrast agent. The result showed a significant ($P < 0.05$) increase in body weight, extensive tumor apoptosis, smaller tumor size, and better accumulation inside tumor tissue for mice treated with activated HA-NLC compared to non-activated NLC and marketed products. It was concluded that HA-NLC promoted the selective targeting and accumulation of Vn inside tumor tissue, prolonging the retention duration and enhancing the drug's cytotoxic effect with increased mice weight as a sign of safety.

Keywords

vinorelbine, nano-lipid carrier (NLC), lung cancer, hyaluronic acid, MRI, SPION

Introduction

Nanostructured lipid carriers (NLC) are typically prepared by combining liquid to solid lipids in a 7:3 ratio, with surfactant content as low as 0.5% (w/v). Compared to solid lipid nanoparticles, the NLC has a less ordered inner structure, resulting in a higher drug-loading possibility and less drug expulsion, and they can incorporate both lipophilic and hydrophilic drugs with the feasibility of providing targeted, sustainable release properties (Gomaa et al. 2022). The conventional NLCs have limitations, such as RES uptake, opsonization, and immunogenicity. So, to overcome such constraints with increasing circulation time, active targeting has been developed, in which several approaches have been adapted for

Copyright *Wannas AN et al.* This is an open access article distributed under the terms of the Creative Commons Attribution License (CC-BY 4.0), which permits unrestricted use, distribution, and reproduction in any medium, provided the original author and source are credited.

PENSOFT

actively targeting a specific body site using ligands to enhance cellular uptake and cytotoxicity (Beloqui et al. 2016).

Hyaluronic acid (HA), which can be used as a ligand for active drug targeting, is a mucopolysaccharide that occurs naturally, consisting of alternatively repeating disaccharide units of N-acetyl-D-glucosamine and D-glucuronic acid. It has a significant role in structural tissue stability and cell growth. In addition, several overexpressed HA receptors are found in cancer cells, such as a cluster of differentiation-44 (CD44), the receptor for hyaluronic acid-mediated motility (RHAMM), and lymphatic vessel-endocytic receptor (LYVE-1). The main difference between tumor and normal cells regarding CD44 receptors is that the endogenously expressed CD44 receptor is found in a low-level and inactive state in normal cells. In contrast, in cancer cells, the CD44 receptors are highly activated and over-expressed on the surface of various tumors, such as lung and breast cancer (Kesharwani et al. 2022).

Imaging techniques are used to visualize targeted therapy's safety and efficacy, and diagnostic tools include computed tomography, positron-emission tomography, magnetic resonance imaging (MRI), and ultrasound. (Lymperopoulos et al. 2017; Zhou et al. 2021). Superparamagnetic iron oxide (SPION) is a contrast agent visualized by magnetic resonance images (MRI). It is well known for its safety, tunable surface, shape, and size. Due to its paramagnetic properties, it is more effective with lower concentrations than other contrast agents, such as gadolinium (Gd). The magnetic resonance signal of SPION gave darker regions that strongly influence T2 spin-spin relaxation times. Its chemical stability, low toxicity, and high magnetic moments make it an excellent choice for biomedical applications (Filippousi et al. 2014; Nelson et al. 2020).

Vinorelbine's aqueous solubility is very low, with high lipid solubility. It is a semisynthetic vinca alkaloid with a broad spectrum of antitumor activity and no selectivity for cancer cells, leading to a serious and wide range of systemic adverse effects. Successful cancer killing by vinorelbine requires long-term exposure and retention in these cells, which is possible through targeted delivery that differentiates normal cancer cells from cancer cells (Gregory and Smith 2000).

Herein, we emphasize the role of HA as a targeting agent for the prepared receptor-mediated NLC for vinorelbine using HA as a ligand on in vitro behavior as well as following its in vivo role to prove the selective accumulation and prolong the retention of the drug in the lung cancer tissue in the hope of enhancing drug efficacy and minimizing its adverse effects.

Materials and methods

Materials

Vinorelbine (Vn) and vinorelbine ditartarate (Vnd) were purchased from Hefei TNJ Chemical company (Anhui, China), 1,2-distearoyl-sn-glycero-3-phosphoethanolamine N-[amino(polyethylene glycol)-2000] (DSPE-PEG_{2000}), DSPE-PEG_{2000}-NH_2, hyaluronic acid (HA) was purchased from Xi'an Ruixi Biotechnology Co, Ltd, (Xi'an, Shaanxi, China), glyceryl monostearate (GMS), octanoic acid oil (OA), soybean lecithin (using parenterally), oleic coated SPION and lutrol F 68 (poloxamer 188) were purchased from Hangzhou Hyper Chemicals Co, Ltd (Gongshu District, Hangzhou, China), Amicon® 15 centrifugal filters and filter syringe (0.22 μm and 0.45 μm), and all other reagents and chemicals were purchased from Sigma-Aldrich Chemie GmbH (Eschenstr. Taufkirchen Germany. Anti-Mcl-1 antibody" (Sino Biological. Cat Num: 106673-T32) and Anti-BAX antibody (Sino Biological. Cat Num: 106076-T38).

Methods

Conjugation of HA with DSPE-PEG_{2000}-NH_2 (DSPE-HA) and characterization

DSPE-HA conjugate was synthesized by mixing 0.131 mmol of hyaluronic acid (HA) in 50 mL of Dimethylformamide solvent using a magnetic stirrer for 10 minutes, then 0.052 mmol of (EDC) 1-ethyl-3-(3-dimethylaminopropyl) carbodiimide was added with continuous stirring for 5 minutes, followed by the addition of 0.052 mmol of N-hydroxysuccinimide (NHS) with continuous stirring by magnetic stirrer at 100 rpm for two hours, after that 0. 026 mmol of DSPE-PEG_{2000}-NH_2 was added with continuous stirring for 48 hours in closed volumetric flask to give the reaction sufficient time to be completed. For the purification of the product (DSPE-HA), the resulting solution was dialyzed using a 10–14 kDa dialysis membrane in deionized DW with frequent changing of deionized DW for efficient side product removal for two days, followed by ultrafiltration using Amicon® 15 mL 10 kDa centrifuged at 4000 rpm for 30 minutes to remove nonconjugated pegylated lipid with HA, and then the product was lyophilized to obtain DSPE-HA conjugate (Surace et al. 2009; Choi et al. 2011). The conjugate was analyzed using ^{1}H NMR (Varian 500 MHz) for characterization.

Preparation of vinorelbine-loaded NLC activated with receptor mediator HA (HA-NLC)

Vinorelbine-loaded HA-NLC (Vn-loaded HA-NLC) was created using the emulsification-ultrasonication method. Briefly, the organic phase was prepared by mixing Vn drug (50 mg) with the optimized quantity of glyceryl monostearate as a lipid (150 mg), octanoic acid as oil (50 mg), and 1% mol of DSPE-HA (60 mg) in a glass beaker with chloroform and ethanol (1:1 ratio), which was then evaporated by hot plate stirrer at 75 °C and 1000 rpm, and melted lipid phase was obtained to which a heated (at 75 °C) aqueous phase containing poloxamer 188 (0.1 w/w%) and soybean lecithin (0.5 w/w%) was added drop by drop. Both were homogenized at 15000 rpm for 5 minutes using a high-speed homogenizer (D 160, Biobase) and then ultrasonicated (UCD 950, Biobase) for 15 minutes (on-off 4-4 sec) to get HA-NLC (Taetz et al. 2009; Liu et al. 2020) (Scheme 1).

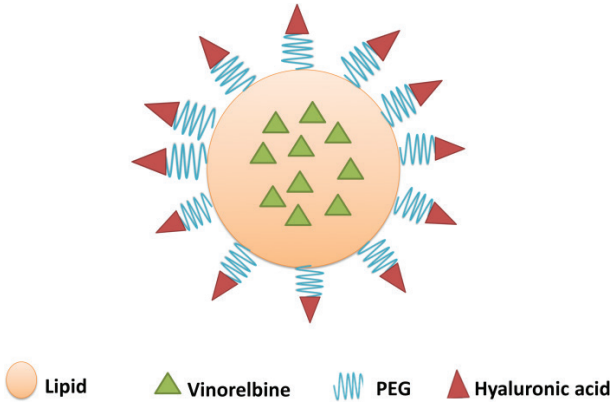

Scheme 1. Orientation of the targeted Vn-loaded HA-NLC, hyaluronic acid nanolipid carrier loaded with vinorelbine (Yang et al. 2018).

Characterization of the prepared Vn-loaded HA-NLC

Particle size, PDI, and zeta potential

The mean particle-size diameter, PDI, and zeta potential of the prepared Vn-loaded HA-NLC were measured using a laser particle size analyzer ABT-9000, USA, for the measurement of PDI and mean particle size, while the zeta potential was measured using Malvern Zeta Sizer, UK. Before the measurement, the samples were diluted with deionized distilled water ten times. All the results were obtained in triplicate (AlEbadi and Al-Lami 2022; Al-Edresi et al. 2024).

Morphology examination for vinorelbine-loaded HA-NLC

Field emission scanning electron microscope (FESEM) was used for the determination of the prepared Vn-loaded HA-NLC morphological characteristics, in which a few drops of diluted formula were added on the surface of an aluminum slab and dried in an oven at 100 °C for few seconds after that, a thin layer of Au/Pd coat was added to the dried samples, which is then observed using different magnifications by FESEM (INSPECT F 50, FEI Company, China) (Ahmed et al. 2021).

In vitro drug release

An in vitro drug release study from the prepared Vn-loaded HA-NLC was performed, in which 10 mL of prepared formula was transferred into a previously soaked (overnight) dialysis membrane with a molecular cut-off of 10–14 kDa. The release study was performed in 400 mL of PBS at 37 °C and 100 rpm for 48 hours, where the samples (3 mL) were continuously removed at predetermined intervals for spectrophotometric analysis (Shimadzu 1800, Japan) at 268 nm and replaced with fresh medium (Wan et al. 2008; Radhi et al. 2023).

In vitro cytotoxicity and MTT assay

The lung cancer cell line (A549) was supplied by the Department of Pharmacology and Toxicology Cell Bank at Mustansiriyah University/College of Pharmacy. Cells were grown in "Roswell Park Memorial Institute (RPMI-1640)" liquid medium (Gibco, UK) supplemented with 10% fetal bovine serum (Gibco, UK). Samples (1 mg/mL) of Vn-loaded HA-NLC, Vn-loaded NLC, and marketed vinorelbine (Navelbine®) were used to prepare serial concentrations (100, 50, 25, 12.5, and 6.25 µg/mL) with (RPMI-1640) media as a diluent (Ashizawa et al. 1993; Obayes et al. 2019).

After different incubation periods (24 h, 48 h, and 72 h), the liquid in the wells was removed, and each well was cleaned with a phosphate-buffered saline (PBS). A 200 µL of 0.5 mg/mL MTT solution was added in each well and then incubated for three hours at 37 °C. At the end of the incubation period, purple-colored intracellular formazan crystals were visible under an inverted microscope. The supernatant was removed, and 100 µL of DMSO was added to each well, which acted as a solvent for the formed formazan crystals. The plate was then incubated at room temperature for 30 minutes to allow the cells to be lysed and the purple crystals to dissolve. The absorbance measurement was achieved at 570 nm using a microplate-ELISA reader (Ghasemi et al. 2021), and this equation calculated the % viability:

$$\%\,\boldsymbol{Viability} = (\boldsymbol{absorbance\ of\ treated\ well}/\boldsymbol{absorbance\ of\ control}) * 100\%$$

In vivo animal study

Animals and tumor models

Thirty mice of the Kunming strain (weighing 20 ± 0.5 g) were purchased from the central animal laboratory of Tehran University of Medical Science (TUMS). All the animals were kept in a pathogen-free environment with reasonable access to food and water at a temperature of 25 ± 2 °C and a relative humidity of 70% ± 5%. The mice were subcutaneously injected with 0.1 mL cell suspension containing LL2 cells (2×10^2 cells/mouse) in the right flank space. LL2 is a highly tumorigenic lung cancer cell line for mice. After seven to fourteen days of tumor inoculation, when the tumor volume approached 100 mm^3, the treatments began, and that day was marked as day 1 (Tran Chau et al. 2020).

The mice (with induced tumors) were classified into six groups (G1–G6), and each group received the assigned solution as in Table 1.

The groups G1–G4 were examined for the survival time, body weight, and change in tumor volume (measured by vernia) every 3 days for four weeks of treatment (Baris et al. 2020; Sahib et al. 2022). All animal experiments were conducted following the guidelines of the Animal Ethical Committee at Mustansiriyah University, College of Pharmacy. The experiment was assigned an ethical code of 19 on 10 Feb. 2024.

Table 1. Mice grouping (G1–G6) according to the study.

Group no.	Treatment
G1	0.2 mL normal saline was given I.V. weekly for four weeks (untreated group).
G2	0.2 mL of marketed vinorelbine (Navelbine®) was given I.V. at a dose of 12 mg/kg weekly for four weeks.
G3	0.2 mL of Vn-loaded NLC was given I.V. at a dose of 12 mg/kg weekly for four weeks.
G4	0.2 mL of Vn-loaded HA-NLC (activated) given I.V. at a dose of 12 mg/kg weekly for four weeks.
G5	0.2 mL of SPION Vn-loaded NLC (SPION NLC) was given I.V. at a dose of 12 mg/kg weekly for four weeks (to be followed by MRI).
G6	0.2 mL of SPION Vn-loaded HA-NLC (SPION HA-NLC) was given I.V. at a dose of 12 mg/kg weekly for four weeks (to be followed by MRI).

Abbreviations: Vn (vinorelbine), NLC (nano-lipid carrier), HA (hyaluronic acid), SPION (superparamagnetic iron oxide).

A contrast agent superparamagnetic iron oxide (SPION) was used for MR imaging and incorporated during NLC formulation, in which 50 mg of oleic-coated SPION was added to the organic phase of Vn-loaded NLC and Vn-loaded HA-NLC and designated as SPION NLC and SPION HA-NLC, then 0.2 mL of each SPION-containing formula was injected I.V. in a dose of 12 mg/kg/week for four weeks in groups G5 and G6. After four weeks, the mice were examined by MRI (Tesla 3 Magnetom Prisma MRI machine in Siemens, Germany) at 0.5, 4, 12, and 24 hours after the injection to estimate the retention of the drug in lung tumor xenograft as well as its clearance (wash-out). The mice during this study were anesthetized by intraperitoneal injection of ketamine (100 mg/kg) and xylazine (10 mg/kg) (the intraperitoneal injections were repeated during the study to ensure continuous anesthesia) (Peira et al. 2003).

Histopathological and Immunohistochemistry (IHC) for lung tumor xenograft

Tumor tissue samples from groups G1–G4 were fixed in 10% formalin, then placed in the block and cast by paraffin (paraffin blocks). Then, for each paraffin block, a microtone was used to get a section of a 7 μm thickness sample and mounted on a positively charged slide. After that, these slides were stained with hematoxylin and eosin (H&E), and a histopathological examination was done using a light microscope (He et al. 2016).

The same procedure was applied for the immunohistochemistry (IHC) study, where three μm-thickness sections were cut from each paraffin block sample and then mounted on positive-charged slides. The first step was deparaffinization by immersing the slides in three xylene containers for 5 minutes. Then, the slides were rehydrated by immersing them for 10 minutes in absolute ethanol, 96% aqueous-ethanol, and 70% aqueous-ethanol solutions sequentially (Magaki et al. 2019).

For the antigen recovery (unmasking) step, the slides were immersed in Tris-EDTA solution for 5 minutes to remove crosslinking that possibly formed during the previous step. Then 100 μL of peroxidase-blocking solution was added to the slides, which were then incubated at room temperature for 60 minutes in a dark-humid chamber. The primary antibody attachment step was then achieved by overnight incubating the slides at 4 °C in a humid chamber with 100 μL of anti-Mcl-1 antibody in a dilution of 1:500 to express BCL2 or anti-BAX antibody in dilution 1:150 to express BAX (BAX and BCL2 are markers for apoptosis) (Frost et al. 2000).

For the identification step of the primary antibody, 100 μL of polymer bound to peroxidase, named as the secondary detection kit, was added to each slide with incubation for 30 minutes at room temperature. After that, the diaminobenzidine "DAB" substrate solution was added to each slide and then incubated in the dark at room temperature for 10 minutes. For nuclei staining, a few drops of hematoxylin were added to each slide as a counter-stain to stain the nuclei of tumor cells with a blue color that provided a contrast to the brown color of the DAB chromogen for better visualization of tissue morphology. The dehydration step of the samples was done by immersing the slides in a sequence series of 70% aqueous ethanol, 96% aqueous ethanol, and 100% absolute ethanol for 1 minute (to protect the artifact-stained slides), followed by immersing them in a xylene container for 5 minutes. The samples were covered with a thin cover glass and examined microscopically using an Amscope optical microscope with 40X magnification. The work was repeated by taking five sections from each group G1–G4 (Y. Li et al. 2018). The data underpinning the analysis reported in this paper are deposited at the "Data Repository" of Zenodo at https://zenodo.org/records/14901728.

Results

Characterization of HA-DSPE

The conjugation of HA with DSPE-PEG_{2000}-NH_2 proceeded through the interaction of primary amine (NH_2) with the carboxyl group of HA, as shown in Scheme 2.

^{1}H-NMR spectrum for HA showed two main chemical shifts for the *N*-acetyl $COCH_3$ group attached with glucosamine rings of HA (δ 1.88 ppm), CH protons of glucosamine, and glucuronic rings of HA (δ 3.20–4.41 ppm) as presented in Fig. 1.

While the ^{1}H-NMR spectrum for DSPE-PEG_{2000}-NH_2 (Fig. 2) showed peaks for CH_3 of the terminal alkyl chain (δ 0.88 ppm), -CH_2 groups of the alkyl chain of DSPE (δ 1.27–1.52 ppm), CH_2 near to the ester moiety of DSPE (δ 2.33–2.79 ppm), the NH_2 group (δ 3.20 ppm), ethyl oxide units of PEG (δ 3.66 ppm), CH_2 group between phosphate and carbonyl group of DSPE (δ 4.16–4.35 ppm), and NH group between phosphate and carbonyl group of DSPE (δ 7.90 ppm).

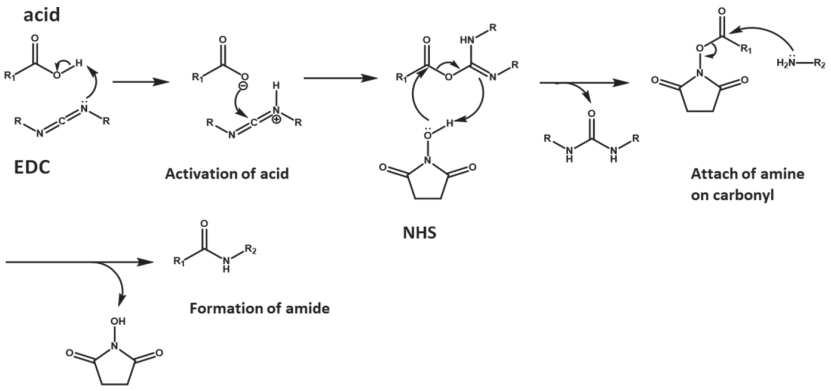

Scheme 2. Conjugation of hyaluronic acid with DSPE-PEG$_{2000}$-NH$_2$ using 1-ethyl-3-(3-dimethylaminopropyl) carbodiimide (EDC) and N-hydroxysuccinimide (NHS) (Iriarte-Mesa et al. 2020).

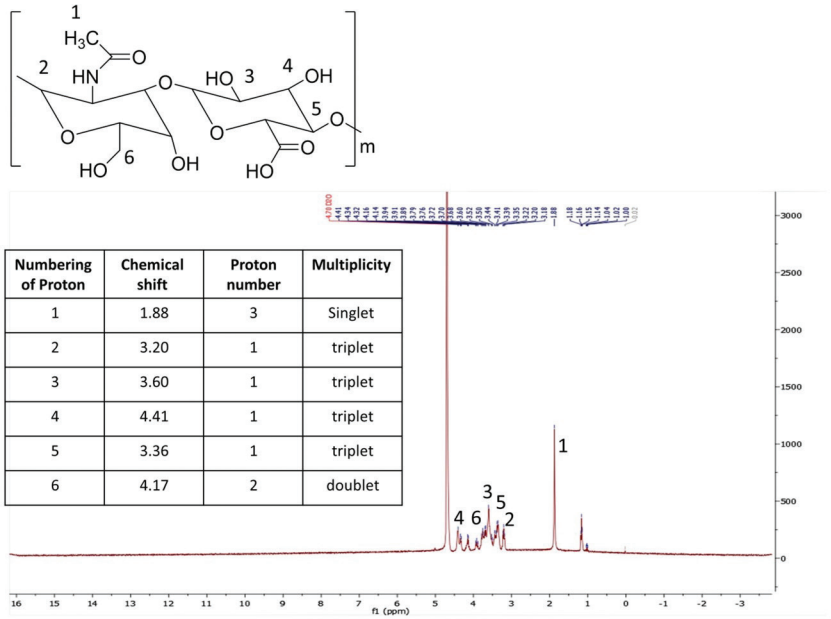

Numbering of Proton	Chemical shift	Proton number	Multiplicity
1	1.88	3	Singlet
2	3.20	1	triplet
3	3.60	1	triplet
4	4.41	1	triplet
5	3.36	1	triplet
6	4.17	2	doublet

Figure 1. ^{1}H-NMR (500 MHz, D_2O) spectrum of hyaluronic acid.

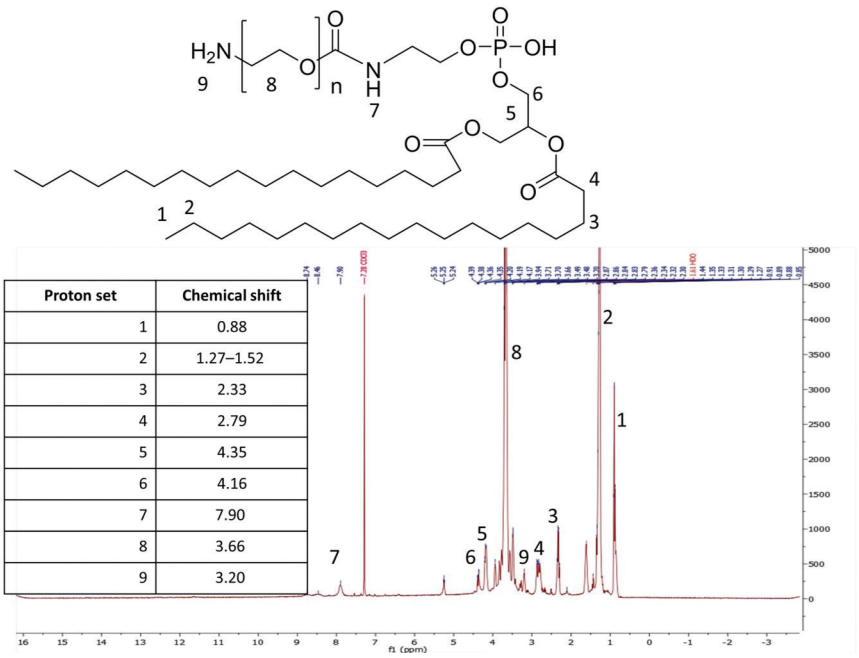

Proton set	Chemical shift
1	0.88
2	1.27–1.52
3	2.33
4	2.79
5	4.35
6	4.16
7	7.90
8	3.66
9	3.20

Figure 2. ^{1}H-NMR (500 MHz, $CDCl_3$) spectrum of DSPE-PEG$_{2000}$-NH$_2$.

The ^{1}H-NMR spectrum of the conjugate (HA-PEG-DSPE) is shown in Fig. 3, in which CH_3 of the terminal alkyl chain (δ 0.88 ppm), -CH_2 groups of the alkyl chain of DSPE (δ 1.27–1.52 ppm), the *N*-acetyl $COCH_3$ group attached with glucosamine rings of HA (δ 1.88 ppm), ethyl oxide units of PEG (δ 3.66 ppm), the NH group between the carbonyl group of the HA moiety and ethyl oxide units of PEG (δ 6.70 ppm), and OH groups of glucosamine and glucuronic rings of HA (δ 3.90–4.21 ppm).

Characterization and evaluation of the prepared Vn-loaded HA-NLC

Particle size, PDI, and zeta potential determination

The prepared Vn-loaded HA-NLC showed a mean particle size of 102 nm, PDI 0.027, and zeta potential of -44.1, as demonstrated in Fig. 4.

Morphological examination of the prepared Vn-loaded HA-NLC formulations by field emission scanning electron microscope (FE-SEM) of HA-NLC

FESEM for the prepared Vn-loaded HA-NLC showed ellipsoidal-shaped particles with a small size, good dispersion without aggregation, and a smooth surface, as shown in Fig. 5.

In vitro drug release

A cumulative drug release from the prepared Vn-loaded HA-NLC is shown in Fig. 6, where a biphasic release was observed, in which an initial release for 40% of drug HA-NLC within 4 h followed by slow release that continued to 85.23% within 48 h.

In vitro cytotoxicity and MTT assay

The results of the MTT assay are presented in Fig. 7 (concentration-response curve) and Fig. 8 (time response curve). The assay measured the % of cell death for marketed vinorelbine (Navelbine®), Vn-loaded NLC, and Vn-loaded HA-NLC at various concentrations (6.25, 12.5, 25, 50, and 100 µg/mL) after 24 h, 48 h, and 72 h post-exposure. In addition, Fig. 9 showed the IC50 of Navelbine® (45.65 µg/mL), Vn-loaded NLC (57.29 µg/mL), and Vn-loaded HA-NLC (35.7 µg/mL).

In vivo animal study

Animals and tumor models

Throughout the 28-day experiment, all mice's tumor size and body weight were continuously measured using a vernier caliper and electronic balance to evaluate the antitumor activity of all vinorelbine samples (marketed vinorelbine Navelbine®, Vn-loaded NLC, and Vn-loaded HA-NLC). The results are presented in Fig. 10.

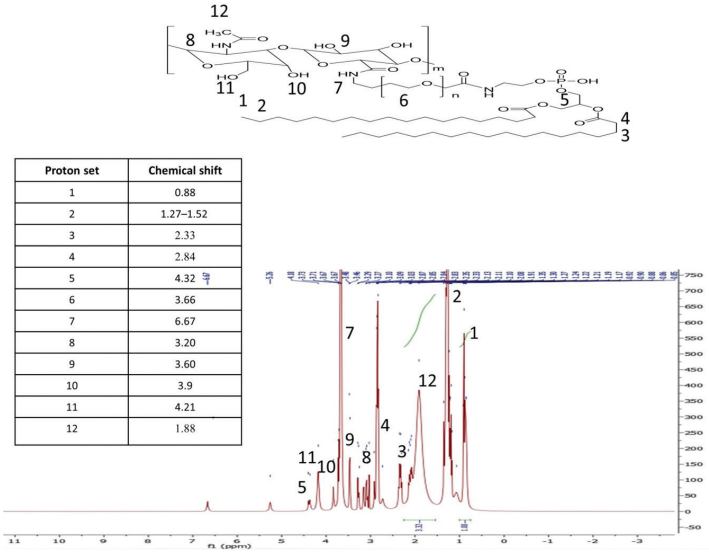

Proton set	Chemical shift
1	0.88
2	1.27–1.52
3	2.33
4	2.84
5	4.32
6	3.66
7	6.67
8	3.20
9	3.60
10	3.9
11	4.21
12	1.88

Figure 3. The ^{1}H-NMR (500 MHz, $CDCl_3$) spectrum of hyaluronic acid conjugated to pegylated-DSPE.

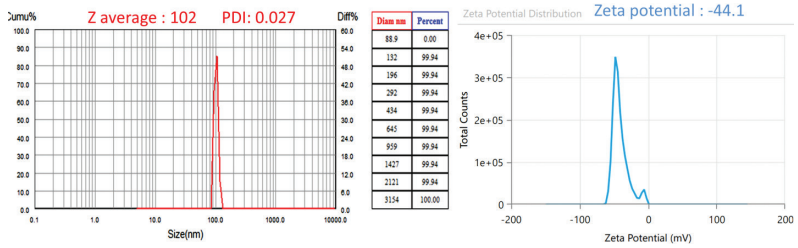

Figure 4. The average particle size, PDI, and zeta potential of Vn-loaded HA-NLC.

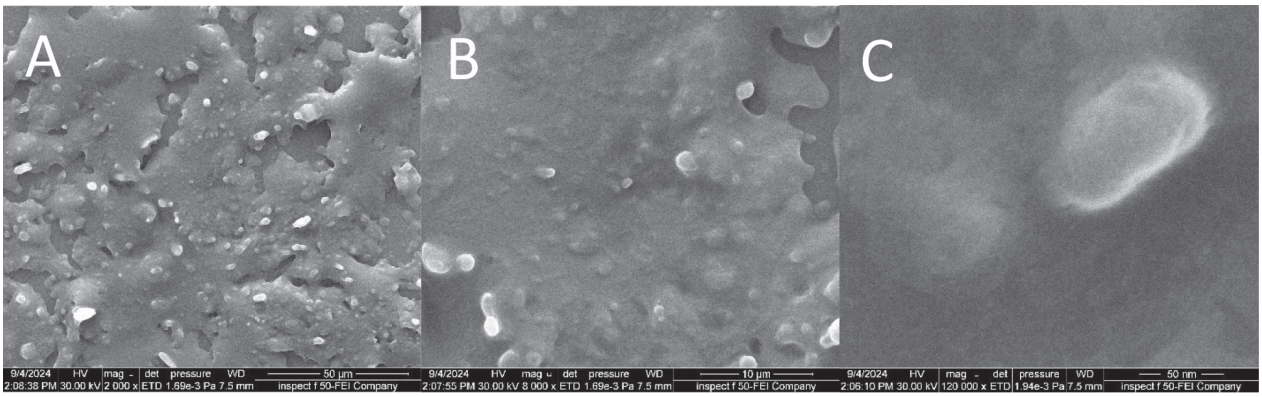

Figure 5. FESEM images of Vn-loaded HA-NLC at **A.** 2000X; **B.** 8000X, and **C.** 120000X magnification.

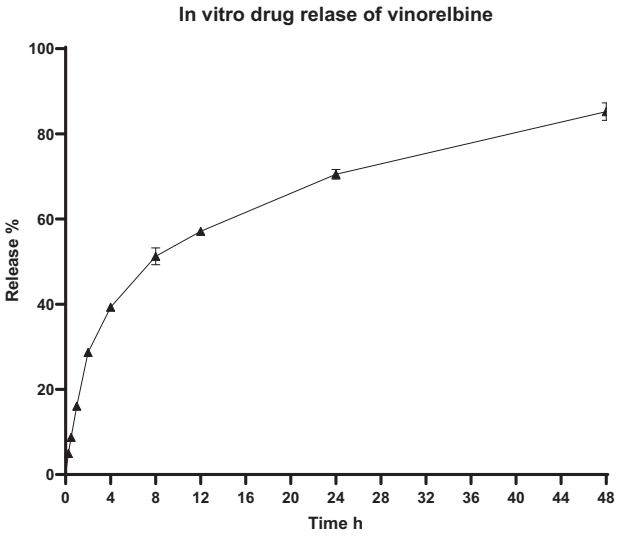

Figure 6. Cumulative release profile of Vn-loaded HA-NLC at pH 7.4.

Concerning groups G5 and G6, where SPION as a contrast agent was included in the formulation of Vn-loaded NLC and Vn-loaded HA-NLC (named SPION NLC and SPION HA-NLC), an MRI scan for the mice in these groups was conducted to follow the accumulation of SPION in the tumor tissue during 24 hours (0.5 h, 4 h, 12 h, and 24 h) after I.V. injection of each formula as presented in Fig. 11.

Histopathological and Immunohistochemistry (IHC) for lung tumor xenograft

The histopathological features, including cell density, morphology, and signs of necrosis or apoptosis using hematoxylin and eosin (HE), were examined using an optical microscope (Fig. 12), in which mice in control group G1 showed the typical characteristics of an untreated tumor, such as high cell density, uniformity, very few or no signs of cell death, lack of immune cell

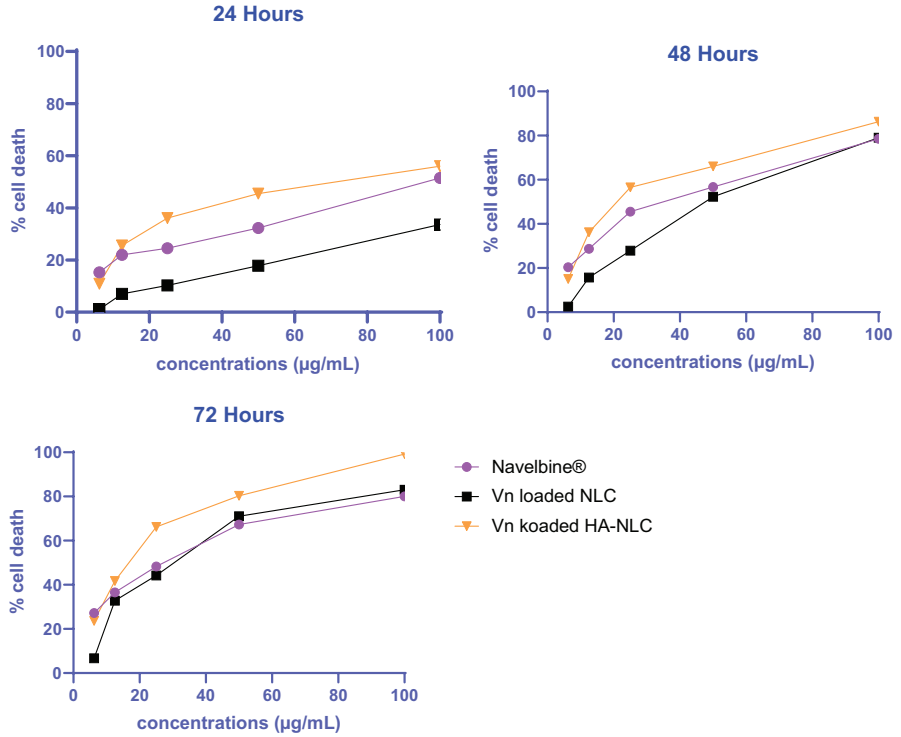

Figure 7. Cell death percentage of the A549 lung cancer cell line for marketed vinorelbine (Navelbine®), Vn-loaded NLC, and Vn-loaded HA-NLC at various concentrations (6.25, 12.5, 25, 50, and 100 µg/mL) at different incubation times: 24 h, 48 h, and 72 h.

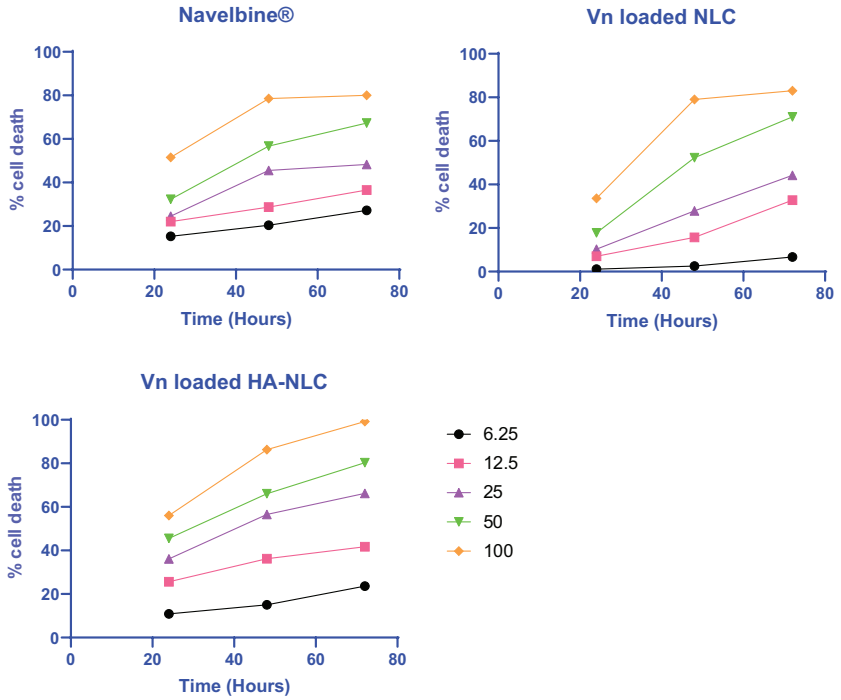

Figure 8. Time-response curves of in vitro cytotoxicity for marketed vinorelbine (Navelbine®), Vn-loaded NLC, and Vn-loaded HA-NLC on the A549 lung cancer cell line.

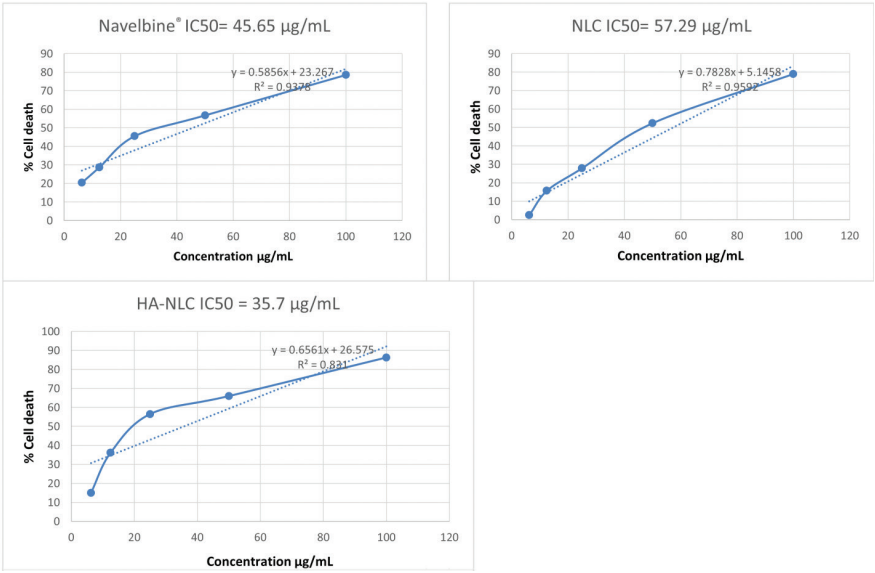

Figure 9. IC50 curves for in vitro cytotoxicity of marketed vinorelbine (Navelbine®), Vn-loaded NLC, and Vn-loaded HA-NLC on the A549 lung cancer cell line.

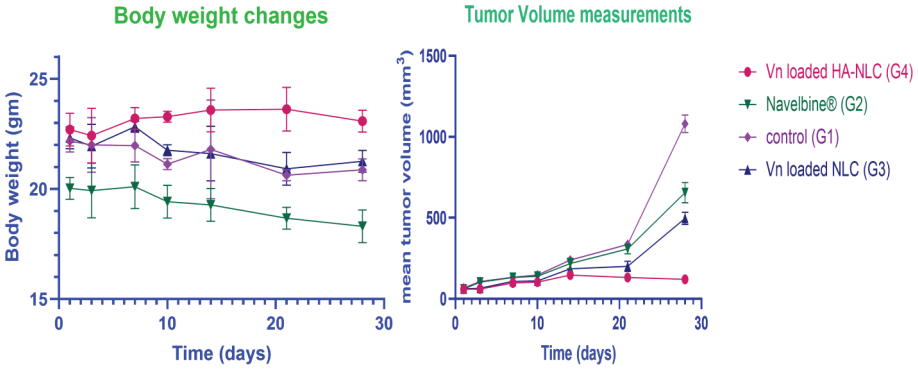

Figure 10. Body weight and tumor volume change in mice for groups (G1-G4).

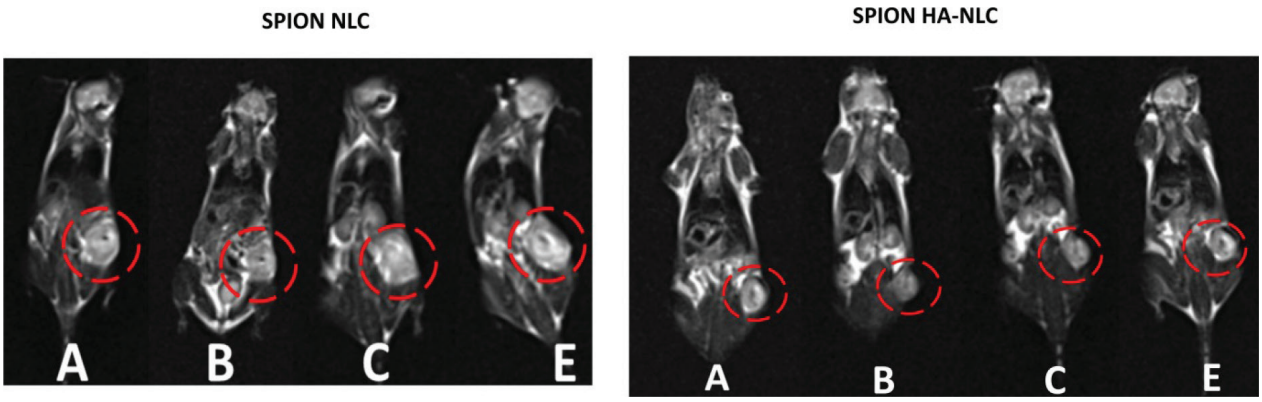

Figure 11. T2-weighted MR images of SPION NLC and SPION HA-NLC in mice groups G5 and G6 after **A.** 0.5 h; **B.** 4 h; **C.** 12 h; and **D.** 24 h post I.V. injection.

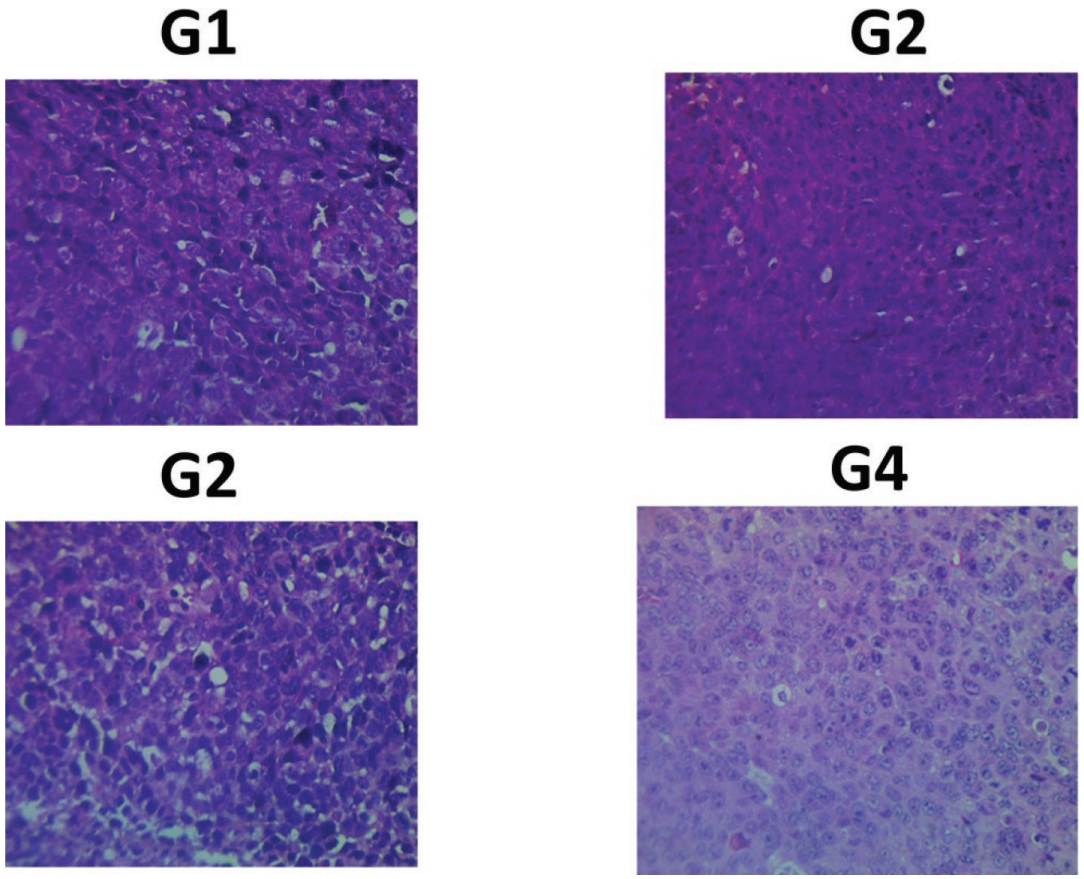

Figure 12. Optical microscope photograph with 40X magnification using hematoxylin and eosin staining for lung cancer tissue in mice groups G1, G2, G3, and G4.

infiltration which is typical for untreated tumor tissue. Navelbine®-treated mice in group G2 showed slightly reduced cellularity compared to control and moderate inflammation around necrotic areas, while Vn-loaded NLC-treated mice in group G3 showed a further reduction in cellular density, more widespread regions of necrosis compared to groups G1 and G2, and fewer mitotic figures. In addition, Vn-loaded HA-NLC-treated mice in group G4 showed shrunken or fragmented cells due to apoptosis, as well as a large area of cell death, with cells losing their structure and becoming eosinophilic (stained pink/red), indicating the presence of immune cells like lymphocytes and macrophages in response to dead tumor cells.

For the immunohistochemistry (IHC) study (Fig. 13, Table 2), the results revealed that apoptosis (represented by BAX) was 4.5 times higher than anti-apoptosis (represented by BCL2) in group G4 treated with receptor-mediated NLC (Vn-loaded HA-NLC), which showed the highest ratio than other groups. The results showed no significant difference ($P > 0.05$) between mice treated with marketed vinorelbine (group G2) and those treated with Vn-loaded NLC (group G3).

The expression status of BAX and BCL2 for lung cancer tissues for groups G1–G4 is presented in Table 2.

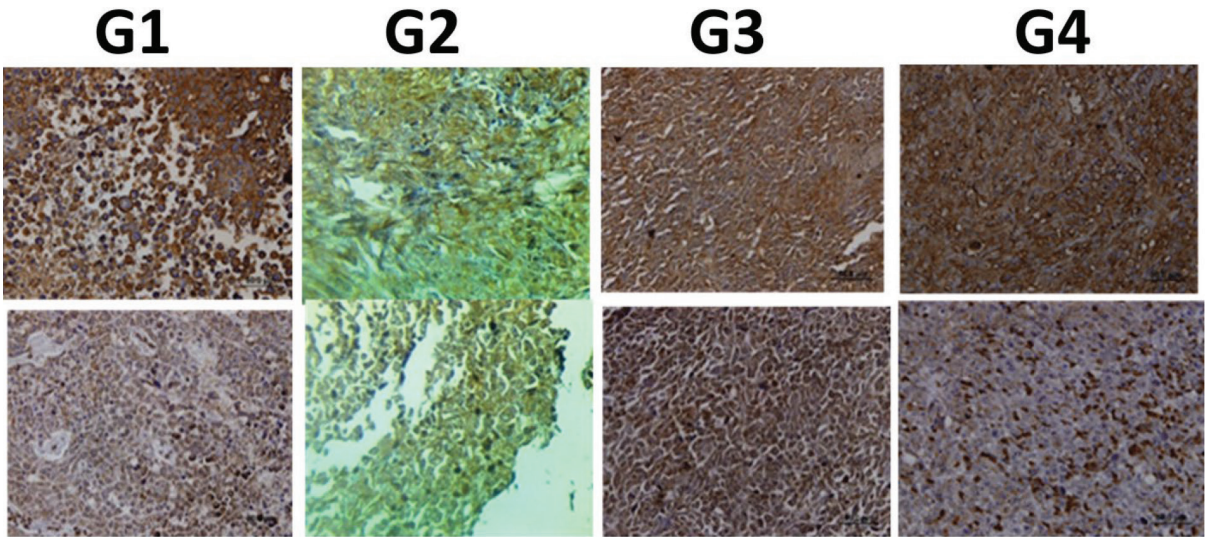

Figure 13. Optical microscope photographs with 40X magnification illustrating BAX and BCL2 expression using the IHC technique for lung cancer tissue in mice groups G1, G2, G3, and G4.

Table 2. Effect of different treatments on BAX and BCL2 expression for lung cancer tissue using five samples for each treated group (G1–G4).

group	parameter	Sample1	Sample2	Sample3	Sample4	Sample5	Mean	Ratio BAX/BCL2
G1	Bax	63	57	52	68	70	62	1.16
	Bcl-2	53	47	46	57	60	53	
G2	Bax	70	78	84	82	85	80	1.42
	Bcl-2	46	57	61	49	67	56	
G3	Bax	58	49	52	44	36	48	1.54
	Bcl-2	41	30	27	35	22	31	
G4	Bax	74	63	81	65	79	72	4.5
	Bcl-2	16	11	21	12	22	16	

Discussion

^{1}H-NMR identification for the conjugation of HA with pegylated DSPE (HA-DSPE)

The average degree of lipid conjugation to the HA backbone monomers was 30%, so the majority of HA (70% of monomers) is free and available for binding to its receptors (CD44). It was calculated based on NMR signals integration at δ 0.88 ppm for CH_3 of the terminal alkyl chain and comparing the integration at δ 1.88 ppm for the *N*-acetyl $COCH_3$ group attached to the glucosamine rings of HA (Lee et al. 2023).

Characterization of the prepared Vn-loaded HA-NLC formulations

Particle size, PDI, and zeta potential

The small particle size and PDI may enhance the diffusion of the drug through the cell and give an indication of uniformity. In addition, the high value of zeta potential reflects excellent thermodynamic stability for the prepared Vn-loaded HA-NLC formula, in which the hyaluronic acid may potentiate the negative charge on the surface of the particle and participate in improving system stability (Yu et al. 2020).

Morphology examination for vinorelbine-loaded HA-NLC

The prepared Vn-loaded HA-NLC showed an ellipsoidal shape that may enhance the penetration of the prepared Vn-loaded HA-NLC through the cell membrane. The particle size measured by FESEM was smaller than that measured by the zeta sizer in which the sample is hydrated, while FESEM involves a prior drying step (Ortiz et al. 2021).

In vitro drug release

The in vitro drug release from the prepared Vn-loaded HA-NLC showed a prolonged release of vinorelbine that continued for 48 h. Such prolonged release could be attributed to the increased diffusion layer around the lipid carrier and the slow partitioning of the drug loaded within the lipid carrier (Kim et al. 2018; Naama et al. 2025).

In vitro cytotoxicity and MTT assay

The results demonstrated that the drug's cytotoxic effect increased with concentration. Also, the time response curve showed that the cytotoxic effect increased with increasing incubation time in all concentrations used (6.25, 12.5, 25, 50, and 100 µg/mL). Within the first 24 h, the marketed vinorelbine (Navelbine®) showed a better cytotoxic effect than

the Vn-loaded NLC formulation, and this was attributed to the slow-release characteristics of the Vn-loaded NLC. At the same time, with Navelbine®, the cells are exposed to a higher drug concentration. However, with a longer exposure duration of 48 h and 72 h, both Navelbine® and Vn-loaded NLC showed higher but non-significant ($P > 0.05$) differences in cell death. The best cytotoxic effect was obtained from the Vn-loaded HA-NLC, which was significantly ($P < 0.05$) higher in all concentrations and time exposures; this could be attributed to the ability of hyaluronic acid to be actively entered into the lung cancer cell through its CD44 receptors, which are commonly available on the surface of the tumor cells (Zhang et al. 2017; Serri et al. 2019), leading to significantly ($P < 0.05$) lower IC50 than those observed with non-activated NLC as well as the marketed one.

In vivo animal study

Animals and tumor models

In this study, mice in group G2 (received the Navelbine®) showed a decline in body weight in the first 3 days that continued to decrease to more than 15% from their original weight at the end of the experiment, which could be related to its gastrointestinal side effects, including anorexia, nausea, and vomiting, which are commonly associated with the use of chemotherapeutic agents. While mice in group G3 (receiving Vn-loaded NLC) showed a slight non-significant ($P > 0.05$) change in mice body weight, and that was possibly related to the enhanced retention and permeation effect of nanosized NLC inside the tumor with the prolonged release characteristic—which might reduce drug side effect—similar results were observed with mice in group G1 (untreated). The best result was observed for group G4, where mice showed an increase in body weight in a more significant ($P < 0.05$) manner than other groups, which may be attributed to the active targeting of tumor cells by Vn-loaded HA-NLC attributed to the binding of HA to the overexpressed CD44 receptors that selectively accumulate the drug to its site of action (Rashid et al. 2020; H. Liu et al. 2024).

Within the first 10 days of starting the experiment, mice in group G4 showed almost the same tumor volume. Still, soft, fluidized tissue indicated improved blood supply to tissue that started upon treatment with vinorelbine from its activated NLC. The result was significantly better than group G3, which further indicated HA's role in the selective accumulation of vinorelbine (Choi et al. 2011; Choi et al. 2011).

Further follow-up for the efficacy of vinorelbine from its HA-activated NLC in comparison to non-activated NLC, an MRI scan was applied to follow the accumulation of SPION (contrast agent) for 24 hours in tumor xenograft for mice in group G5 (treated with vinorelbine loaded in SPION NLC) and group G6 (treated with Vn loaded in SPION HA-NLC). Group G6 showed a high accumulation of the contrast agent in tumor tissue represented by a darker tumor region through the measurement of T2 spin-spin relaxation times. This further supported the selective delivery of vinorelbine to the tumor tissue in vivo from its HA-activated NLC compared to non-activated NLC (Li et al. 2014; Hu et al. 2018).

Histopathological and immunohistochemistry (IHC) for lung tumor xenograft

For histopathological use of hematoxylin and eosin (HE), the result of the control group (G1) indicated active proliferation with irregular nuclear shapes and sizes, suggesting malignancy and some areas of necrosis and inflammation. The Navelbine®-treated group (G2) showed evidence of cell death (necrosis) compared to group G1 due to vinorelbine's cytotoxic effect. Vn-loaded NLC-treated group (G3) showed reduced tumor proliferation with increased inflammatory response, potentially due to more tumor cell deaths caused by the enhanced tissue retention and permeation effects of the NLC with extended drug release, resulting in longer exposure duration. In contrast, the Vn-loaded HA-NLC-treated group (G4) showed a larger area of apoptosis and changes in cellular structure in comparison to other groups, which could be attributed to targeting a high concentration of drug at a tumor tissue site due to hyaluronic acid-mediated endocytosis by the major CD44 receptors and other hyaluronic receptors that are over-expressed on the surface of tumor cancer (Varghese et al. 2014; Spadea et al. 2019). The IHC study also confirmed these results.

Conclusion

Preparing activated NLC through conjugation with hyaluronic acid as a ligand affects the drug's in vitro and in vivo behavior, leading to improved diffusion and prolonging the retention duration of vinorelbine by increasing the accumulation of the drug inside tumor tissue. The utilization of SPION as a contrast agent further proves the role of HA and follows up on the selective targeting of the drug to tumor tissue. Such accumulation and targeting enhanced the cytotoxic effect of the drug with a possible significant reduction in side effects.

Acknowledgment

The authors thank Mustansiriyah University (www.uomustansiriyah.edu.iq) for supporting the work.

Additional information

Conflict of interest

The authors have declared that no competing interests exist.

Ethical statements

The authors declared that no clinical trials were used in the present study.

The authors declared that no experiments on humans or human tissues were performed for the present study.

The authors declared that no informed consent was obtained from the humans, donors or donors' representatives participating in the study.

Experiments on animals: 19 on 10th Feb. 2024.

Use of commercially available immortalised human and animal cell lines: The lung cancer cell line (A549) was supplied by the Department of Pharmacology and Toxicology Cell Bank at Mustansiriyah University/College of Pharmacy.

Funding

No funding was reported.

Author contributions

All authors have contributed equally.

Author ORCIDs

Ali N. Wannas https://orcid.org/0000-0002-1563-7026
Monther F. Mahdi https://orcid.org/0000-0002-2069-4121
Nidhal K. Maraie https://orcid.org/0000-0001-5628-1479

Data availability

All of the data that support the findings of this study are available in the main text.

References

Ahmed S, Mahmood S, Ansari MD, Gull A, Sharma N, Sultana Y (2021) Nanostructured lipid carrier to overcome stratum corneum barrier for the delivery of agomelatine in rat brain; formula optimization, characterization and brain distribution study. International Journal of Pharmaceutics 607: 121006. https:/doi.org/10.1016/j.ijpharm.2021.121006

Al-Edresi S, Hamrah KA, Al-Shaibani A (2024) Formulation and validation of Candesartan cilexetil-loaded nanosuspension to enhance solubility. Pharmacia 71: 1–13. https://doi.org/10.3897/pharmacia.71.e114943

AlEbadi NN, Al-Lami MS (2022) Formulation and in-vitro evaluation of ethosomes using anastrozole as a modeling drug. Al mustansiriyah journal of pharmaceutical sciences 22(4): 90–105. https://doi.org/10.32947/ajps.v22i4.971

Ashizawa T, Miyoshi K, Asada M, Kobayashi E, Okabe M, Morimoto M, Hirata T (1993) Antitumor activity of navelbine (vinorelbine ditartrate), a new vinca alkaloid analog. Gan to kagaku ryoho. Cancer & chemotherapy 20(1): 59–66. https://doi.org/10.1097/00001813-199412000-00004

Baris MM, Serinan E, Calisir M, Simsek K, Aktas S, Yilmaz O, Secil M (2020) Xenograft tumor volume measurement in nude mice: estimation of 3D ultrasound volume measurements based on manual caliper measurements. Journal of Basic and Clinical Health Sciences 4(2): 90–95. https://doi.org/10.30621/jbachs.2020.902

Beloqui A, Solinís MÁ, Rodríguez-Gascón A, Almeida AJ, Préat V (2016) Nanostructured lipid carriers: Promising drug delivery systems for future clinics. Nanomedicine: Nanotechnology, biology and medicine 12(1): 143–161. https://doi.org/10.1016/j.nano.2015.09.004

Choi KY, Min KH, Yoon HY, Kim K, Park JH, Kwon IC, Jeong SY (2011) PEGylation of hyaluronic acid nanoparticles improves tumor targetability in vivo. Biomaterials 32(7): 1880–1889. https://doi.org/10.1016/j.biomaterials.2010.11.010

Choi KY, Yoon HY, Kim JH, Bae SM, Park RW, Kang YM, Park JH (2011) Smart nanocarrier based on PEGylated hyaluronic acid for cancer therapy. ACS nano 5(11): 8591–8599. https://doi.org/10.1021/nn202070n

Filippousi M, Angelakeris M, Katsikini M, Paloura E, Efthimiopoulos I, Wang Y, Van Tendeloo G (2014) Surfactant effects on the structural and magnetic properties of iron oxide nanoparticles. The Journal of Physical Chemistry C 118(29): 16209–16217. https://doi.org/10.1021/jp5037266

Frost A R, Sparks D, Grizzle W E (2000) Methods of antigen recovery vary in their usefulness in unmasking specific antigens in immunohistochemistry. Applied Immunohistochemistry & Molecular Morphology 8(3): 236–243. https://doi.org/10.1097/00129039-200009000-00011

Ghasemi M, Turnbull T, Sebastian S, Kempson I (2021) The MTT assay: utility, limitations, pitfalls, and interpretation in bulk and single-cell analysis. International journal of molecular sciences 22(23): 12827. https://doi.org/10.3390/ijms222312827

Gomaa E, Fathi HA, Eissa NG, Elsabahy M (2022) Methods for preparation of nanostructured lipid carriers. Methods 199: 3–8. https://doi.org/10.1016/j.ymeth.2021.05.003

Gregory RK, Smith IE (2000) Vinorelbine–a clinical review. British journal of cancer 82(12): 1907–1913. https://doi.org/10.1054/bjoc.2000.1203

He H, Yang Y, Xiang Z, Yu L, Chouitar J, Yu J, Tirrell S (2016) A Sensitive IHC Method for Monitoring Autophagy- Specific Markers in Human Tumor Xenografts. Journal of Biomarkers 2016(1): 1274603. https://doi.org/10.1155/2016/1274603

Hu Y, Mignani S, Majoral JP, Shen M, Shi X (2018) Construction of iron oxide nanoparticle-based hybrid platforms for tumor imaging and therapy. Chemical Society Reviews 47(5): 1874–1900. https://doi.org/10.1039/C7CS00657H

Iriarte-Mesa C, López,Y C, Matos-Peralta Y, de la Vega-Hernández K Antuch M (2020) Gold, silver and iron oxide nanoparticles: synthesis and bionanoconjugation strategies aiming to electrochemical applications. Surface-modified nanobiomaterials for electrochemical and biomedicine applications, 93–132. https://link.springer.com/article/10.1007/s41061-019-0275-y

Kesharwani P, Chadar R, Sheikh A, Rizg WY, Safhi AY (2022) CD44-targeted nanocarrier for cancer therapy. Frontiers in pharmacology 12: 800481. https://doi.org/10.3389/fphar.2021.800481

Kim CH, Sa CK, Goh MS, Lee ES, Kang TH, Yoon HY, Choi YW (2018) pH-sensitive PEGylation of RIPL peptide-conjugated nanostructured lipid carriers: Design and in vitro evaluation. International journal of nanomedicine 2018(13): 6661–6675. https://doi.org/10.2147/IJN.S184355

Lee CE, Kim S, Park HW, Lee W, Jangid AK, Choi Y, Kim K (2023) Tailoring tumor-recognizable hyaluronic acid–lipid conjugates to enhance anticancer efficacies of surface-engineered natural killer cells. Nano Convergence 10(1): 56. https://doi.org/10.1186/s40580-023-00406-1

Li J, He Y, Sun W, Luo Y, Cai H, Pan Y, Shi X (2014) Hyaluronic acid-modified hydrothermally synthesized iron oxide nanoparticles for targeted tumor MR imaging. Biomaterials 35(11): 3666–3677. https://doi.org/10.1016/j.biomaterials.2014.01.011

Li Y, Li N, Yu X, Huang K, Zheng T, Cheng X, Liu X (2018) Hematoxylin and eosin staining of intact tissues via delipidation and ultrasound.

Scientific reports 8(1): 12259. https://doi.org/10.1038/s41598-018-30755-5

Liu H, Li M, Lin Y, You H, Kou J, Feng W (2023) Dual-directional effect of vinorelbine combined with cisplatin or fluorouracil on tumor growth and metastasis in metronomic chemotherapy in breast cancer. International Journal of Oncology 64(2): 13. https://doi.org/10.3892/ijo.2023.5601

Liu X, Liu H, Wang SL, Liu JW (2020) Hyaluronic acid derivative-modified nanostructured lipid carrier for cancer targeting and therapy. Journal of Zhejiang University. Science B 21(7): 571. https://doi.org/10.1631/jzus.b1900624

Lymperopoulos G, Lymperopoulos P, Alikari V, Dafogianni C, Zyga S, Margari N (2017) Application of theranostics in oncology. In: Vlamos P (Ed.) GeNeDis 2016. Advances in Experimental Medicine and Biology, vol 989. Springer, Cham., 119–128. https://doi.org/10.1007/978-3-319-57348-9_10

Magaki S, Hojat S A, Wei B, So A, Yong W H (2019) An introduction to the performance of immunohistochemistry, 289–298. Springer New York. https://doi.org/10.1007/978-1-4939-8935-5_25

Naama NA, Hameed GS, Hanna DB, Mahdi ZH (2025) Formulation of Cefdinir Ternary Solid Dispersion and Stability Study under Harsh Conditions. Al Mustansiriyah Journal of Pharmaceutical Sciences 25(1): 27–48. https://10.0.128.179/2c6tqn40

Nelson NR, Port JD, Pandey MK (2020) Use of superparamagnetic iron oxide nanoparticles (SPIONs) via multiple imaging modalities and modifications to reduce cytotoxicity: An educational review. Journal of Nanotheranostics 1(1): 105–135. https://doi.org/10.3390/jnt1010008

Obayes SK, Obied HN, Al-Saadi MA (2019) An in vitro Study for the Synergistic Cytotoxic Actions of Biological Therapy and Anticancer Chemotherapy. Prof. RK Sharma 13(3): 242. https://doi.org/10.5958/0973-9130.2019.00202.0

Ortiz AC, Yañez O, Salas-Huenuleo E, Morales JO (2021) Development of a nanostructured lipid carrier (NLC) by a low-energy method, comparison of release kinetics and molecular dynamics simulation. Pharmaceutics 13(4): 531. https://doi.org/10.3390/pharmaceutics13040531

Peira E, Marzola P, Podio V, Aime S, Sbarbati A, Gasco MR (2003) In vitro and in vivo study of solid lipid nanoparticles loaded with superparamagnetic iron oxide. Journal of Drug Targeting 11(1): 19–24. https://doi.org/10.1080/1061186031000086108

Radhi AA, Ali WK, Al-Saedi F (2023) Tamoxifen Citrate-loaded synthetic high-density lipoproteins: Assessment of cellular toxicity in breast cancer cells. Al Mustansiriyah Journal of Pharmaceutical Sciences 23(1): 58–67. https://doi.org/10.32947/ajps.v23i1.987

Rashid MM, Lee H, Jung BH (2020) Evaluation of the antitumor effects of PP242 in a colon cancer xenograft mouse model using comprehensive metabolomics and lipidomics. Scientific Reports 10(1): 17523. https://doi.org/10.1038/s41598-020-73721-w

Sahib AS, Wennas ON, Mahdi BW (2022) In vivo antitumor activity study of targeted chlorambucil-loaded nanolipid carrier for breast cancer. Pharmacia 69(3): 631–636. https://doi.org/10.3897/pharmacia.69.e85390

Serri C, Quagliariello V, Iaffaioli RV, Fusco S, Botti G, Mayol L, Biondi M (2019) Combination therapy for the treatment of pancreatic cancer through hyaluronic acid- decorated nanoparticles loaded with quercetin and gemcitabine: A preliminary in vitro study. Journal of cellular physiology 234(4): 4959–4969. https://doi.org/10.1002/jcp.27297

Spadea A, Rios de la Rosa JM, Tirella A, et al. (2019) Evaluating the efficiency of hyaluronic acid for tumor targeting via CD44. Molecular Pharmaceutics 16(6): 2481–2493. https://doi.org/10.1021/acs.molpharmaceut.9b00083

Surace C, Arpicco S, Dufaÿ-Wojcicki A, Marsaud V, Bouclier C, Clay D, Fattal E (2009) Lipoplexes targeting the CD44 hyaluronic acid receptor for efficient transfection of breast cancer cells. Molecular pharmaceutics 6(4): 1062–1073. https://doi.org/10.1021/mp800215d

Taetz S, Bochot A, Surace C, Arpicco S, Renoir JM, Schaefer UF, Fattal E (2009) Hyaluronic acid-modified DOTAP/DOPE liposomes for the targeted delivery of anti-telomerase siRNA to CD44-expressing lung cancer cells. Oligonucleotides 19(2): 103–116. https://doi.org/10.1089/oli.2008.0168

Tran Chau V, Liu W, Gerbé de Thoré M, Meziani L, Mondini M, O'Connor M J, Clémenson C (2020) Differential therapeutic effects of PARP and ATR inhibition combined with radiotherapy in the treatment of subcutaneous versus orthotopic lung tumour models. British Journal of Cancer 123(5): 762–771. https://doi.org/10.1038/s41416-020-0931-6

Varghese F, Bukhari AB, Malhotra R, De A (2014) IHC Profiler: an open source plugin for the quantitative evaluation and automated scoring of immunohistochemistry images of human tissue samples. PLoS ONE 9(5): e96801. https://doi.org/10.1371/journal.pone.0096801

Wan F, You J, Sun Y, Zhang XG, Cui FD, Du YZ, Hu FQ (2008) Studies on PEG-modified SLNs loading vinorelbine bitartrate (I): preparation and evaluation in vitro. International journal of pharmaceutics 359(1–2): 104–110. https://doi.org/10.1016/j.ijpharm.2008.03.030

Yang F, Li A, Liu H, Zhang H (2018) Gastric cancer combination therapy: synthesis of a hyaluronic acid and cisplatin containing lipid prodrug coloaded with sorafenib in a nanoparticulate system to exhibit enhanced anticancer efficacy and reduced toxicity. Drug design, development and therapy, 3321–3333. https://doi.org/10.2147/DDDT.S176879

Yu T, Li Y, Gu X, Li Q (2020) Development of a hyaluronic acid-based nanocarrier incorporating doxorubicin and cisplatin as a pH-sensitive and CD44-targeted anti-breast cancer drug delivery system. Frontiers in Pharmacology 11: 532457. https://doi.org/10.3389/fphar.2020.532457

Zhang B, Zhang Y, Yu D (2017) Lung cancer gene therapy: Transferrin and hyaluronic acid dual ligand-decorated novel lipid carriers for targeted gene delivery. Oncology reports 37(2): 937–944. https://doi.org/10.3892/or.2016.5298

Zhou J, Rao L, Yu G, Cook TR, Chen X, Huang F (2021) Supramolecular cancer nanotheranostics. Chemical Society Reviews 50(4): 2839–2891. https://doi.org/10.1039/D0CS00011F